Science of the Total Environment 626 (2018) 244–254

Contents lists available at ScienceDirect

Science of the Total Environment

journal homepage: www.elsevier.com/locate/scitotenv

Long-term trend analysis on total and extreme precipitation over Shasta Dam watershed

Kinya Toride [a,*], Dylan L. Cawthorne [a], Kei Ishida [a], M. Levent Kavvas [a], Michael L. Anderson [b]

[a] Department of Civil and Environmental Engineering, University of California, Davis, 1 Shields Ave, Davis, CA 95616, United States
[b] California Department of Water Resources, Sacramento, CA, United States

HIGHLIGHTS

- Total and extreme precipitation over Shasta greatly increased during 1851 to 2010.
- No significant trends in precipitation totals and extremes are found after the mid-1900s.
- Precipitation trends at watershed-scale and regional scale may be different.
- The variability of annual precipitation has significantly increased since 1970s.
- Integrated water management is becoming crucial over the Shasta Dam watershed.

GRAPHICAL ABSTRACT

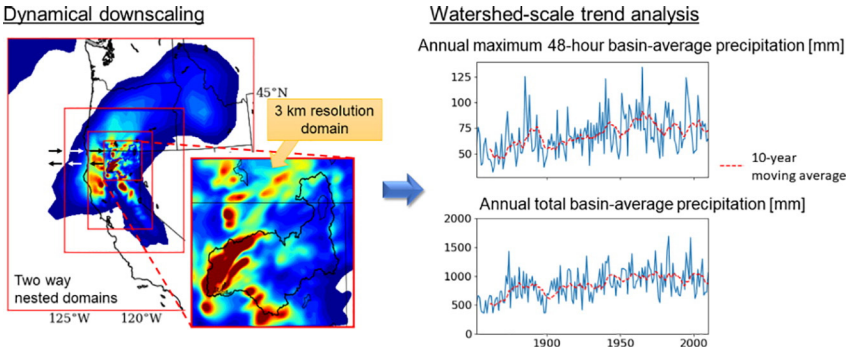

ARTICLE INFO

Article history:
Received 11 November 2017
Received in revised form 31 December 2017
Accepted 1 January 2018
Available online 19 February 2018

Editor: D. Barcelo

Keywords:
Climate change analysis
Dynamical downscaling
Historical precipitation
Watershed-scale trend analysis

ABSTRACT

California's interconnected water system is one of the most advanced water management systems in the world, and understanding of long-term trends in atmospheric and hydrologic behavior has increasingly being seen as vital to its future well-being. Knowledge of such trends is hampered by the lack of long-period observation data and the uncertainty surrounding future projections of atmospheric models. This study examines historical precipitation trends over the Shasta Dam watershed (SDW), which lies upstream of one of the most important components of California's water system, Shasta Dam, using a dynamical downscaling methodology that can produce atmospheric data at fine time-space scales. The Weather Research and Forecasting (WRF) model is employed to reconstruct 159 years of long-term hourly precipitation data at 3 km spatial resolution over SDW using the 20th Century Reanalysis Version 2c dataset. Trend analysis on this data indicates a significant increase in total precipitation as well as a growing intensity of extreme events such as 1, 6, 12, 24, 48, and 72-hour storms over the period of 1851 to 2010. The turning point of the increasing trend and no significant trend periods is found to be 1940 for annual precipitation and the period of 1950 to 1960 for extreme precipitation using the sequential Mann-Kendall test. Based on these analysis, we find the trends at the regional scale do not necessarily apply to the watershed-scale. The sharp increase in the variability of annual precipitation since 1970s is also detected, which implies an increase in the occurrence of extreme wet and dry conditions. These results inform long-term planning decisions regarding the future of Shasta Dam and California's water system.

© 2018 Elsevier B.V. All rights reserved.

* Corresponding author.
E-mail address: ktoride@ucdavis.edu (K. Toride).

https://doi.org/10.1016/j.scitotenv.2018.01.004
0048-9697/© 2018 Elsevier B.V. All rights reserved.

1. Introduction

Recent climate change has been influencing the climate system both at local and continental scales. Precipitation is one atmospheric variable that has been changing along with the global temperature rise. It is generally reported that wet areas have become wetter and dry areas have become drier (Dore, 2005), and extreme precipitation events have intensified over the 20th century (Alexander et al., 2006; Groisman et al., 2005; O'Gorman, 2015). Min et al. (2011) identified the increase in observed daily heavy precipitation is due to anthropogenic effects in two-thirds of Northern Hemisphere land areas. The global average rate of increase in extreme precipitation was found to be 5.9% to 7.7% per K of near-surface temperature, which is similar to the Clausius-Clapeyron relationship (Westra et al., 2013). Understanding the behavior of precipitation under changing climate is critical as it can cause catastrophic economic damage through floods and droughts.

A number of studies have shown that there has been an increase in heavy precipitation in the United States (Higgins et al., 2007; Karl and Knight, 1998; Kunkel et al., 2013). Annual precipitation depth was found to be increased by 10% across the United States during 1910 to 1995, which increase is mainly due to the change in heavy precipitation (Karl and Knight, 1998). However, identified trends in extreme precipitation in the west coast of the United States by several studies have been inconclusive. According to Kunkel et al. (2013), there is no significant trends in 2-day extreme precipitation in the western United States over the periods of 1895–2010 and 1957–2010 based on gauge data from the National Weather Service Cooperative Observer network. Pryor et al. (2009) reported slight increases in 90th and 95th percentiles daily precipitation over the 20th century, though there were limited number of rainfall gauges in the western states. On the other hand, Mass et al. (2011) examined 2-day extreme precipitation for 1950–2009 along the coastal zone of the United States and found a decreasing trend from northern California through the central Oregon coast.

The spatially heterogeneous pattern of temporal trends in heavy precipitation is due to the high spatiotemporal variability of precipitation. To estimate reliable statistical trends in extremes, spatially-averaged heavy precipitation over a spatially homogeneous region should be analyzed (Groisman et al., 2005). Watershed-scale analysis is one possible solution for this purpose, and it is generally the scale where the needs of local agencies and dam operators are. It is also geographically meaningful to conduct trend analysis at the watershed-scale since hydrologic responses caused by storm events would be confined within watersheds (Cheung et al., 2008).

When conducting trend analysis on precipitation, time series data are either obtained from long-term precipitation gauge observations (Kiely, 1999; Saidi et al., 2013) or historically reconstruction by climate simulations (Groisman et al., 2005; Schär et al., 2016). While gauge observation data are commonly used in trend analysis at the watershed-scale, precipitation gauging stations in many watersheds around the world are only available at coarse spatial resolutions and often placed at low elevations in their watersheds, which contributes to an underestimation of precipitation due to the orographic effect. On the other hand, many studies have been reconstructed atmospheric fields by assimilating observed data into climate models (Compo et al., 2011; Kanamitsu et al., 2002; Saha et al., 2006; Toride et al., 2017c). The historical datasets obtained from global climate models are useful to examine a general breadth of precipitation change, but downscaling methods are required to analyze precipitation at the watershed-scale in order to account for the effect of the local topography.

Dynamical downscaling, which nests a regional climate model into a coarse-resolution atmospheric dataset to obtain a finer resolution climatic dataset, is an alternative way to assess watershed-scale climate trend analysis (Ishida et al., 2017; Trinh et al., 2017b). Due to the increasing reliability of dynamical downscaling, it overwhelms traditional statistical downscaling approaches in estimating extreme precipitation (Maraun et al., 2010; Westra et al., 2014). Moreover, the methodology allows studying long-term trends of sub-daily precipitation using historical reanalysis data (Ishida and Kavvas, 2016), which would be difficult otherwise given the limited availability of high-quality rainfall observations. It is also possible to apply the method to estimate future trends in watershed-scale precipitation using future climate projections as done by Ishida et al. (2017). Another thing to note in this study is that trends in precipitation may be different over different watersheds in California in the future, indicating the importance of trend analysis at the watershed-scale. In addition, the reconstructed atmospheric data would facilitate studying historical streamflow patterns by providing the derived dataset to hydrological models (Kavvas et al., 2012; Kure et al., 2013).

This study aims to derive insights into long-term historical precipitation trends over the Shasta Dam watershed (SDW) in northern California. SDW is chosen as the study watershed because SDW is one of the most vital components in California's water system. Recently, Trinh et al. (2016) implemented the fifth-generation Mesoscale Model (MM5) (Grell et al., 1994) and the Watershed Environmental Hydrology model (WEHY) (Chen et al., 2004; Kavvas et al., 2004) over SDW, and reconstructed historical precipitation and water supply information during 1950–2000. By applying the coupled model to future projections, it was found that snow water content would decrease and severity and duration of drought would increase over SDW during the 21st century (Trinh et al., 2017a, b).

Thus, the main objective of this study is to investigate possible climate change in the past over SDW given the changes under future climate projections. A long-term historical reanalysis dataset, the 20th Century Reanalysis Version 2c (20CRv2c) (Compo et al., 2011) is utilized in this study because such a data's length allows long-term reconstruction of atmospheric data beginning from 1851, which would be a longer-time analysis than the previous regional trend analysis studies in California. The methodology uses a physically-based model to dynamically downscale historical reanalysis data from 2° to 3 km spatial resolution to recreate atmospheric fields during the study period. This study reconstructs long-term precipitation data over SDW with an hourly temporal resolution for 159 years to recognize trends that have implications for the future management of water and anthropogenic resources, since it would elucidate the precipitation trend in the important watershed where no concrete conclusions have been derived. In California, many of the hourly gauging observation stations became available during the last two decades, and the stations within mountainous watersheds are not distributed spatially well enough to represent basin-average precipitation (Ishida and Kavvas, 2016). This approach, compared with gauging observations, may be able to provide reliable trend analysis based on more consistent precipitation fields over SDW.

2. Study area and data

2.1. Study area

SDW is chosen for this study because of Shasta Dam's significance to California's water system. It has an area of 19,212 km^2 and is located in a mountainous region with elevation ranging from 308 to 4206 m. The dominant land covers over the study watershed are evergreen forest (52%), shrubland (24%), and grassland (10%) according to the National Land Cover Database. Behind Shasta Dam lies Shasta Lake, the largest single man-made reservoir in California, with a capacity of about 5.6 billion cubic meters. The continued proper management of seasonally-dependent water supply behind Shasta Dam is one of the main motivations of this study. Flood control is also a major function of Shasta Dam and a motivator for a precipitation trend analysis over SDW. California's Mediterranean climate means that precipitation in the winter months poses a risk of flooding, and flooding in the Sacramento River watershed has been observed as far back as the Great Flood of 1862 (Engstrom,

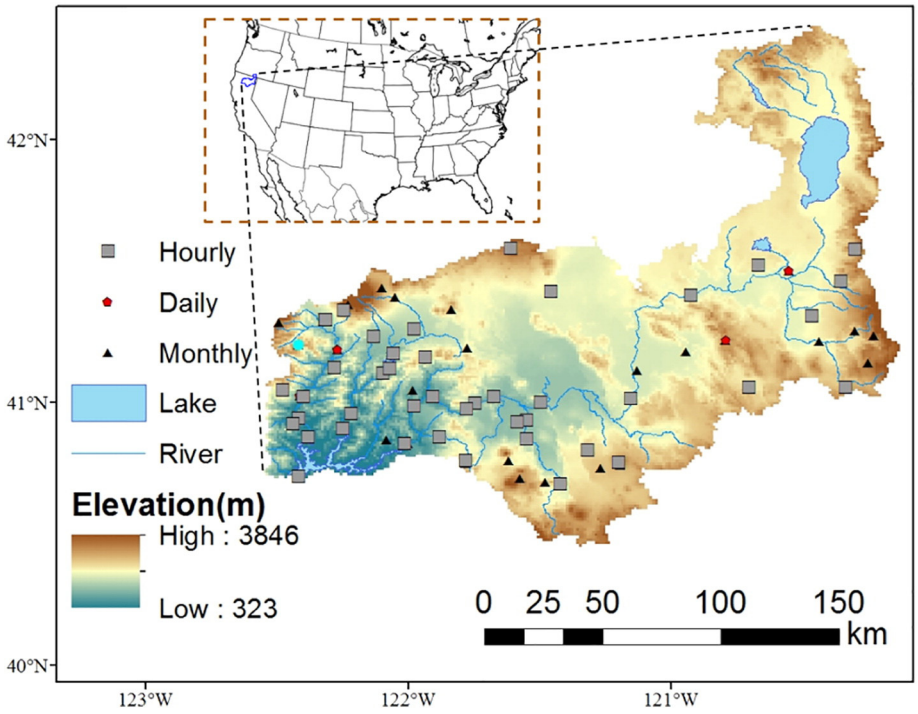

Fig. 1. The Shasta Dam Watershed with the locations of rainfall gauges obtained from the California Data Exchange Center. Surface elevation is quantified by the US Geological Survey National Elevation Dataset. The figure within the red dashed box shows the location of the target watershed (blue line) over the US.

1996). A precipitation trend study such as the current one could offer insights into policies needed to address changes in flood frequency and severity at Shasta Dam. A map of SDW is found in Fig. 1.

The cause of precipitation events in northern California is often atmospheric rivers (ARs), or high moisture flows, coming from the Pacific Ocean (Dettinger et al., 2011; Ralph et al., 2006; Toride et al., 2017b). A single AR can have a greater moisture flux than that of the Amazon River, the largest river on Earth (Zhu and Newell, 1998). The cause of these ARs is thought to be the warm phase of the El Niño Southern Oscillation, often referred to as El Niño. Prolonged warmer-than-normal sea surface temperatures in the central and east-central equatorial Pacific Ocean are indicative of El Niño events, and these warm temperatures often supply extra moisture and energy into the atmosphere, causing ARs. This study acknowledges ARs as the source of much of the precipitation that falls over SDW, but does not attempt to ascertain trends in El Niño occurrences.

2.2. Data

An atmospheric dataset is required to run a regional atmospheric model such as WRF. A reanalysis dataset called 20CRv2c developed by a collaboration between the Physical Sciences Division (PSD) of the Earth System Research Laboratory (ESRL) in NOAA and the Cooperative Institute for Research in Environmental Sciences (CIRES) is used in this study (Compo et al., 2011). This dataset spans from 1851 to present at a six-hourly temporal resolution and 2.0° spatial resolution, and uses surface and sea level pressure observations along with short-term forecasts to produce estimates of atmospheric conditions. The relatively long timeframe of this dataset enables simulation of weather events and validation of model results over the entire 20th century and halfway into the 19th century, thus allowing the analysis of long-term precipitation trends.

The observation data used to evaluate the accuracy of the WRF model output is gridded Parameter-elevation Relationships on Independent Slopes Model (PRISM) data from the PRISM Climate Group at Oregon State University (http://prism.oregonstate.edu/) (Daly et al., 2008). This dataset gathers observations from monitoring networks around the country, and uses a weighted regression to interpolate climate data based on topographic and physiographic variables. Monthly-timescale PRISM data are available from 1895 to present, and daily-timescale PRISM data are available from 1981 to present. Both monthly and daily-timescale precipitation data at 3 km resolution are used in the validation of this study's results.

3. Method

To analyze the aspects of how precipitation over SDW changes over time, a long-term historical precipitation dataset is reconstructed using the dynamical downscaling method. From the reconstructed dataset, time series of basin-average total precipitation and extreme precipitation are calculated over the entire period. In this study, annual maximum values of six different time increments are utilized to analyze trends in extreme precipitation. Several statistical tests are used to detect trends and trend change point years in precipitation over SDW during 1851–2010. Furthermore, the spatial structure of precipitation trends is analyzed by taking advantage of the dynamical downscaling method. Lastly, the variability of annual precipitation is analyzed in order to link the result with recent extreme climate conditions in California.

3.1. Dynamical downscaling

In order to analyze the long-term 20CRv2c dataset over a watershed, it is necessary to downscale to a sufficiently fine spatial resolution. The Weather Research and Forecasting (WRF) model (Skamarock et al., 2008) is employed to simulate precipitation over SDW over the study period. Four two-way nested domains are created in the WRF model to dynamically downscale atmospheric data to 3 km resolution. A map projecting these domains over California geography and SDW is found in Fig. 2. The four domains have 24 × 22 horizontal grid points at 81 km resolution, 37 × 31 horizontal grid points at 27 km resolution, 73 × 49 horizontal grid points at 9 km resolution, and 88 × 85 horizontal

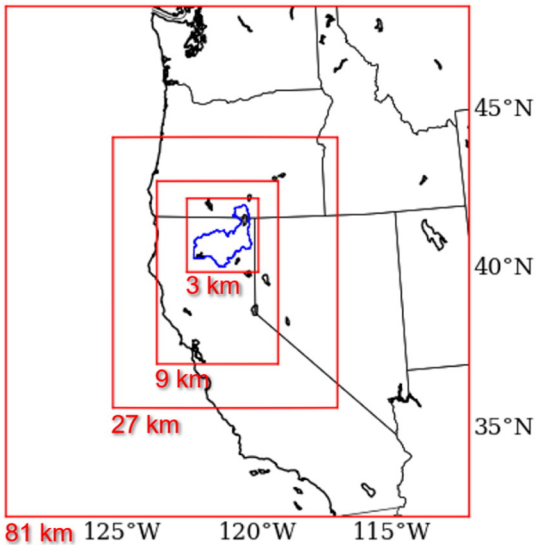

Fig. 2. Depiction of nested 81, 27, 9, and 3 km resolution model domains over the Shasta Dam Watershed (blue line) used for the Weather Research and Forecasting model.

grid points at 3 km resolution, respectively, with 25 vertical levels. The 3 km run is primarily used in the analysis.

The parameterization options of the WRF model are selected based on the comparisons of the model simulations with the corresponding PRISM data in water year 1997, which spans from October 1, 1996 to September 31, 1997. Water year 1997 is used because the two months period of December to January of 1996–1997 saw one of the larger floods in Northern California's history (Halpert and Bell, 1997). Nash-Sutcliffe efficiency (NSE) coefficient is used to evaluate the accuracy of the WRF model output. Based on the evaluation, the Stony Brook University scheme (Lin and Colle, 2011) for microphysics, the New Goddard scheme (Chou and Suarez, 1999) for longwave and shortwave radiation physics, the Bougeault-Lacarrere Planet Boundary Layer scheme (Bougeault and Lacarrere, 1989) for planetary boundary layer physics, the New Simplified Arakawa-Schubert scheme (Han and Pan, 2011) for cumulus parameterization, and the Noah Land Surface Model (Niu et al., 2011) for land surface physics are chosen (Toride et al., 2017a). Fig. 3 provides the comparison of simulated and PRISM daily basin-average precipitation in water year 1997. The NSE between simulated and PRISM data is 0.82, validating the above-mentioned configuration of the WRF model for this study.

Using the previous mentioned domains and physics parameterization options, historical hourly precipitation at 3 km spatial resolution over SDW is reconstructed from 1 October 1851 to 30 September 2010. Basin-average precipitation is then calculated for the whole period in order to analyze precipitation trends over SDW. The simulated basin-average precipitation is validated through the PRISM data in the following section.

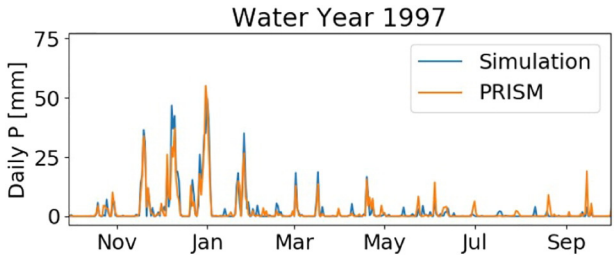

Fig. 3. Time series of simulated and PRISM daily basin-average precipitation over the Shasta Dam Watershed from 1 October 1996 to 30 September 1997.

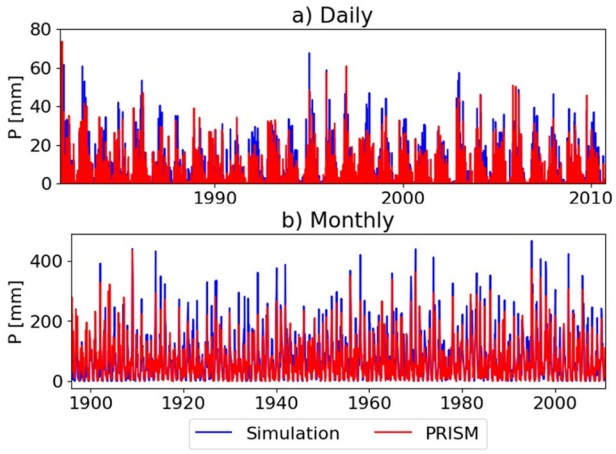

Fig. 4. Time series of simulated and PRISM (a) daily, and (b) monthly basin-average precipitation over the Shasta Dam Watershed.

3.2. Validation

Fig. 4 shows the evaluation of the reconstructed precipitation field with the PRISM data, where hourly precipitation output is aggregated into days and then months for comparisons. Basin-average precipitation, simulated by the configured WRF model, is validated in all the whole available periods of the PRISM data, namely water years 1982–2010 for daily data and water years 1895–2010 for monthly data. The calculated statistics over the periods are summarized in Table 1. The NSE is 0.55 and the correlation coefficient is 0.83 in the daily validation, indicating that model has a relatively good estimation of daily precipitation back to the beginning of water year 1982. A comparison of the simulated versus observed daily precipitation also reveals that the model consistently overestimates the mean and standard deviation of precipitation. This phenomenon can also be seen in Fig. 4, which visually confirms that the peaks of the simulated precipitation are higher than the PRISM precipitation.

The NSE of 0.74 and the correlation coefficient of 0.92 in the monthly validation are strong indicators that the WRF model output matches that of the PRISM observation data (Table 2). Comparison with the daily validation shows that both statistical measures of the model's accuracy (coefficient of correlation and NSE) improve when a longer and coarser temporal-resolution dataset is used. This speaks to the ability of longer-term datasets to better capture climate phenomena. Also, similar to the daily-timescale validation, the WRF model predicts a higher monthly mean for precipitation than the PRISM observation data.

Although the reconstructed precipitation tends to be consistently higher than the PRISM data, uncertainties lie in PRISM as well (see the Discussion section). It is common to correct systematic biases in regional climate models against observation data for hydrological applications. Monthly bias-correction, nested bias-correction, and quantile mapping techniques are the three common techniques to correct the statistics of downscaled precipitation (Sachindra et al., 2014). The

Table 1
Statistics between simulated and PRISM basin-average precipitation. The daily data are evaluated from 1 October 1981 to 30 September 2010, and monthly data are evaluated from October 1895 to September 2010.

	Daily		Monthly	
	PRISM	Reconstructed	PRISM	Reconstructed
Mean [mm]	2.27	2.66	67.0	75.8
STD [mm]	5.29	6.32	67.9	81.7
Correlation	0.831		0.918	
NSE	0.553		0.743	

STD: standard deviation, NSE: Nash-Sutcliffe efficiency.

Table 2
p-Values of Mann–Kendall trend test, Kendall's τ statistics, Theil-Sen slope β, and trend in percentage of annual and monthly basin-average precipitation from water year 1852 to water year 2010. The trend in percentage is calculated based on the Theil-Sen slope and the mean annual or monthly basin-average precipitation during 1852–2010.

	Jan	Feb	Mar	Apr	May	Jun	Jul	Aug	Sep	Oct	Nov	Dec	Annual
p-Value	0.044	0.0027	0.013	2.1×10^{-5}	0.0024	8.0×10^{-5}	0.08	9.6×10^{-6}	0.0043	0.0046	0.045	0.049	5.5×10^{-9}
τ	0.108	0.160	0.132	0.228	0.162	0.211	0.094	0.237	0.153	0.152	0.107	0.105	0.312
β [mm/yr]	0.320	0.411	0.266	0.302	0.165	0.132	0.018	0.025	0.020	0.129	0.214	0.299	2.61
Trend [%/yr]	0.208	0.303	0.226	0.423	0.306	0.438	0.187	0.458	0.223	0.319	0.235	0.221	0.306

quantile mapping is considered to be more appropriate for correcting daily precipitation, though it alters the trends of precipitation. Since we are more interested in the trends than the absolute values of precipitation, no bias-correction is applied in this study to retain the coherent structure of the WRF output.

3.3. Trend analysis

We first investigate the trends in annual and monthly basin-average precipitation over SDW for 159 years. Then, the trends in extreme precipitation with six time-windows are analyzed. Annual basin-average precipitation is calculated using the water year definition in order to include consecutive precipitation events in a calendar year. The nonparametric Mann-Kendall trend test (Kendall, 1948; Mann, 1945) is performed to assess if there is a monotonic upward or downward trend of precipitation over time. The Mann-Kendall test evaluates whether to reject the null hypothesis (H_0) and accept the alternative hypothesis (H_a) where H_0 indicates no monotonic trend and H_a indicates that a monotonic trend is present. The *p* values are calculated as two-sided and the test is performed at a 0.05 significance level. Kendall's τ, which is a normalized statistic ranging between −1 and 1, is used to detect whether the trend is upward or downward. This test has been widely used to examine trends in hydro-meteorological data (Kunkel et al., 2013; Villarini et al., 2009; Westra et al., 2013).

Let a precipitation time series $x = \{x_1, x_2, \ldots, x_n\}$. The Mann-Kendall test statistic S is given by

$$S = \sum_{k=1}^{n-1} \sum_{j=k+1}^{n} sgn(x_j - x_k) \tag{1}$$

where $sgn(x_j - x_k)$ is the sign function of $(x_j - x_k)$. The test statistic S represents the number of times x_j is greater than x_k minus the number of times x_k is greater than x_j, where $j > k$. Thus, if S is positive, the time series tends to be larger with time. The variance of S is

$$var(S) = \frac{n(n-1)(2n+5) - \sum_{k=1}^{m} t_k(t_k-1)(2t_k+5)}{18} \tag{2}$$

where m is the number of the tied groups in the time series, and t_k is the number of ties in the kth tied group. The normalized test statistic is calculated as

$$Z = \begin{cases} \dfrac{S-1}{\sqrt{var(S)}}, & \text{if } S>0 \\ 0, & \text{if } S = 0 \\ \dfrac{S+1}{\sqrt{var(S)}}, & \text{if } S<0 \end{cases} \tag{3}$$

Subsequently, the Kendall's τ is obtained as follows:

$$\tau = \frac{S}{\sqrt{\left(\dfrac{n(n-1)}{2} - \sum_{k=1}^{m} \dfrac{t_k(t_k-1)}{2}\right)\left(\dfrac{n(n-1)}{2}\right)}} \tag{4}$$

where the equation is derived based on the assumption that there are no tied values in time.

A simple least squares estimation is not appropriate to quantify the magnitude of trends if the data are not Gaussian distributed. In this study, we use the Theil-Sen estimator proposed by Sen (1968) to account for the nonnormality of precipitation data. In this approach, $N = n(n-1)/2$ sets of slope estimates are first calculated. The slope Q_{ij} for $1 \le i \le j \le n$ is

$$Q_{ij} = \frac{x_j - x_i}{j - i} \tag{5}$$

Then, by ranking N values of Q_{ij} in ascending order and denoting kth smallest value as Q_k for $k = 1, 2, \ldots, N$, the nonparametric estimate of the slope is obtained as

$$\beta = \begin{cases} Q_{(N+1)/2}, & \text{if } N \text{ is odd} \\ (Q_{N/2} + Q_{(N+2)/2})/2, & \text{if } N \text{ is even} \end{cases}$$

In this study, β is used to express the precipitation change [mm] per year. It is also used to estimate a percent change with respect to the mean annual or extreme precipitation during a certain period.

Additionally, the sequential Mann-Kendall test (Sneyers et al., 1998) is employed to detect the period when a change of trend may occur. Let a precipitation time series $x = \{x_1, x_2, \ldots, x_n\}$. The progressive and retrograde rank series $u(t_i)$ and $u'(t_{i+1})$ are obtained from performing the Mann-Kendall tests on the subseries $\{x_1, \ldots, x_i\}$ and $\{x_{i+1}, \ldots, x_n\}$ for $i = 1, \ldots, n$, respectively. The absolute values of $u(t_i)$ and $u'(t_{i+1})$ correspond to standardized trend statistics Z of the Mann-Kendall test. If the absolute value exceeds 1.96, the null hypothesis is rejected at a 0.05 significance level.

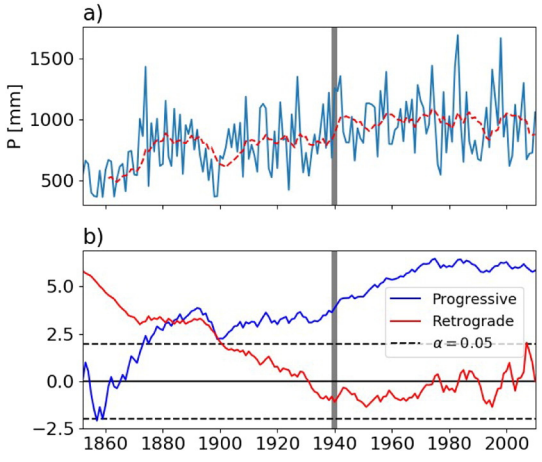

Fig. 5. Annual precipitation and its trend analysis. a) Time series of reconstructed annual basin-average precipitation (blue) and its 10-year moving average (red dashed). b) The sequential Mann-Kendall test on annual basin-average precipitation. Blue and red lines show the progressive and retrograde rank series, respectively. Dashed line corresponds to the 0.05 significance level. The vertical gray-shaded area in both figures indicates the period of transition estimated by the Mann-Kendall test.

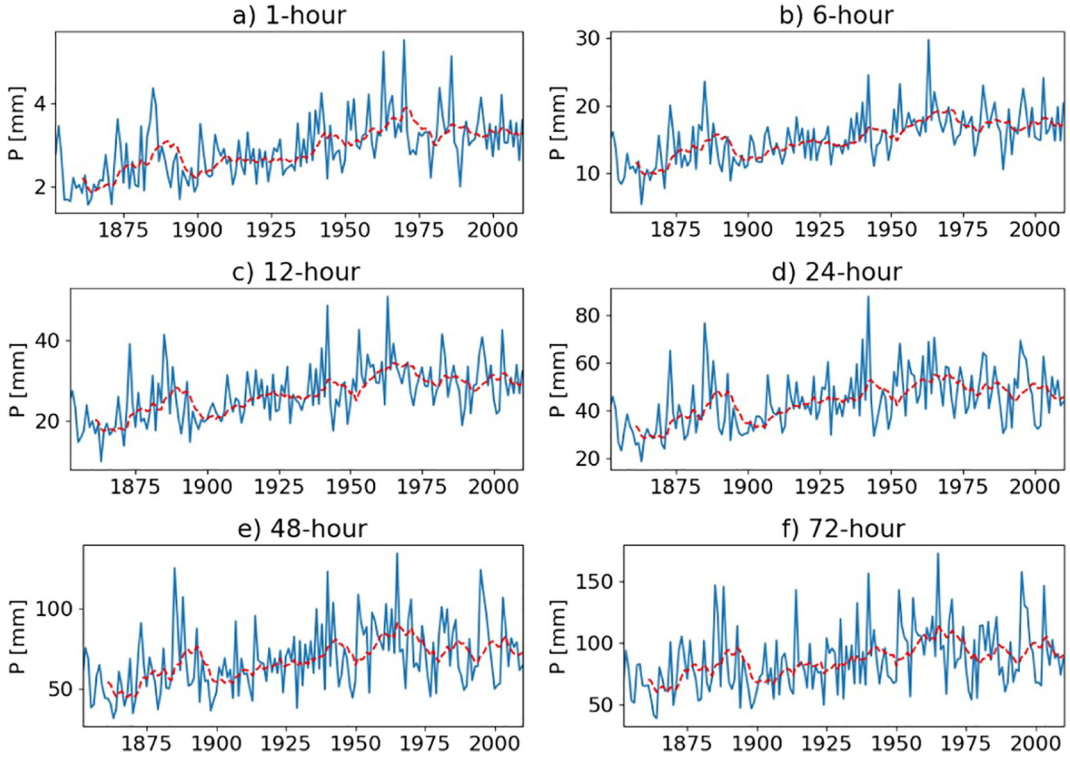

Fig. 6. Annual maximum 1, 6, 12, 24, 48, and 72-hour basin-average precipitation (blue) and its 10-year moving average (red dashed) over the Shasta Dam Watershed.

4. Results

The general trend of precipitation over SDW is analyzed on annual scale. Fig. 5a shows the time series of annual basin-average precipitation in water years 1852–2010 estimated by dynamical downscaling of 20CRV2c dataset. While it seems that there is no significant trend in recent years, the 10-year moving average of precipitation is increasing over the whole period. This trend is consistent with the peak and bottom values as well in Fig. 5a. This increasing trend over the whole period is found to be statistically significant ($p = 5.5 \times 10^{-9}$) by the Mann-Kendall test as shown in Table 2. According to the Theil-Sen estimator, it has increased by 48.7% during the 159-year period.

The seasonality of trends in precipitation is studied by monthly precipitation. It is found that the trend in annual precipitation also applies to monthly basin-average precipitation. The increasing trends of monthly precipitation over the period of 1852 to 2010 are statistically significant ($p < 0.05$) except July as provided in Table 2. While most of precipitation falls during November to March over SDW, July is generally the driest month (approximately 70% of annual precipitation falls during November to March, and <1% of annual precipitation falls in July according to the basin-average PRISM monthly data). This fact indicates that the upward trend is dominant in monthly precipitation over SDW.

Although the increase in annual basin-average precipitation is statistically significant during the period of 1852 to 2010, it can be observed that the 10-year moving average of annual basin-average precipitation is not increasing in the recent period as observed from Fig. 5a. Thus, the sequential Mann-Kendall test is applied to examine when did the increasing trend settle down. Fig. 5b shows the progressive and retrograde rank series of basin-average annual precipitation. The progressive rank series grows rapidly and surpasses the 0.05 confidence level, suggesting that any subseries beginning in 1852 has a statistically significant upward trend. Please note that we do not consider the trend of data shorter than 30 years. However, the retrograde rank series exhibits that annual precipitation has no significant trend over the recent years. Potential trend turning points are estimated when the progressive or retrograde series show changes in their systematic increase or decrease (Sneyers et al., 1998). From the estimates, the increasing trend of annual precipitation transits to a stable condition around 1940. The period of transition is shown by the vertically shaded area in Fig. 5. The increasing trend is significant in the period during 1852 to 1940 ($p = 4.41 \times 10^{-5}$, $\tau = 0.293$), and no significant trend is found in the period during 1941 to 2010 ($p = 0.40$, $\tau = -0.069$).

The dynamical downscaling methodology allows studying the trends of extreme precipitation since it produces fine temporal resolution data. Here annual maximum values of 1, 6, 12, 24, 48, and 72-hour basin-average precipitation over SDW have been calculated for 159 water years. Fig. 6 shows the time series of the annual maximum values. Except for the 24-hour maximum basin-average precipitation, the largest depth for each duration occurred after 1960. The minimum depths of annual maximum values are observed in either 1863 or 1864 and have never fallen below. Moreover, the 10-year moving averages in Fig. 6 provide a basic visualization of upward trends in extreme precipitation in SDW. Every Mann-Kendall trend test performed on extreme events rejected the null hypothesis as seen in Table 3. It is noted that Kendall's τ and the trend in percentage during 1852–2010 increase as the duration of the storm decreases except for hourly maximums,

Table 3
p-Values of Mann–Kendall trend test, Kendall's τ statistics, Theil-Sen slope β, and trend in percentage of annual maximum 1-, 6-, 12-, 24-, 48-, and 72-hour basin-average precipitation from water year 1852 to water year 2010. The trend in percentage is calculated based on the Theil-Sen slope and the mean annual maximum values during 1852–2010.

	1 h	6 h	12 h	24 h	48 h	72 h
p-Value	3.13×10^{-14}	2.66×10^{-15}	1.63×10^{-13}	2.50×10^{-10}	2.82×10^{-7}	1.66×10^{-5}
τ	0.406	0.422	0.394	0.388	0.275	0.234
β [mm/yr]	0.009	0.046	0.081	0.126	0.169	0.18
Trend [%/yr]	0.294	0.306	0.304	0.288	0.247	0.203

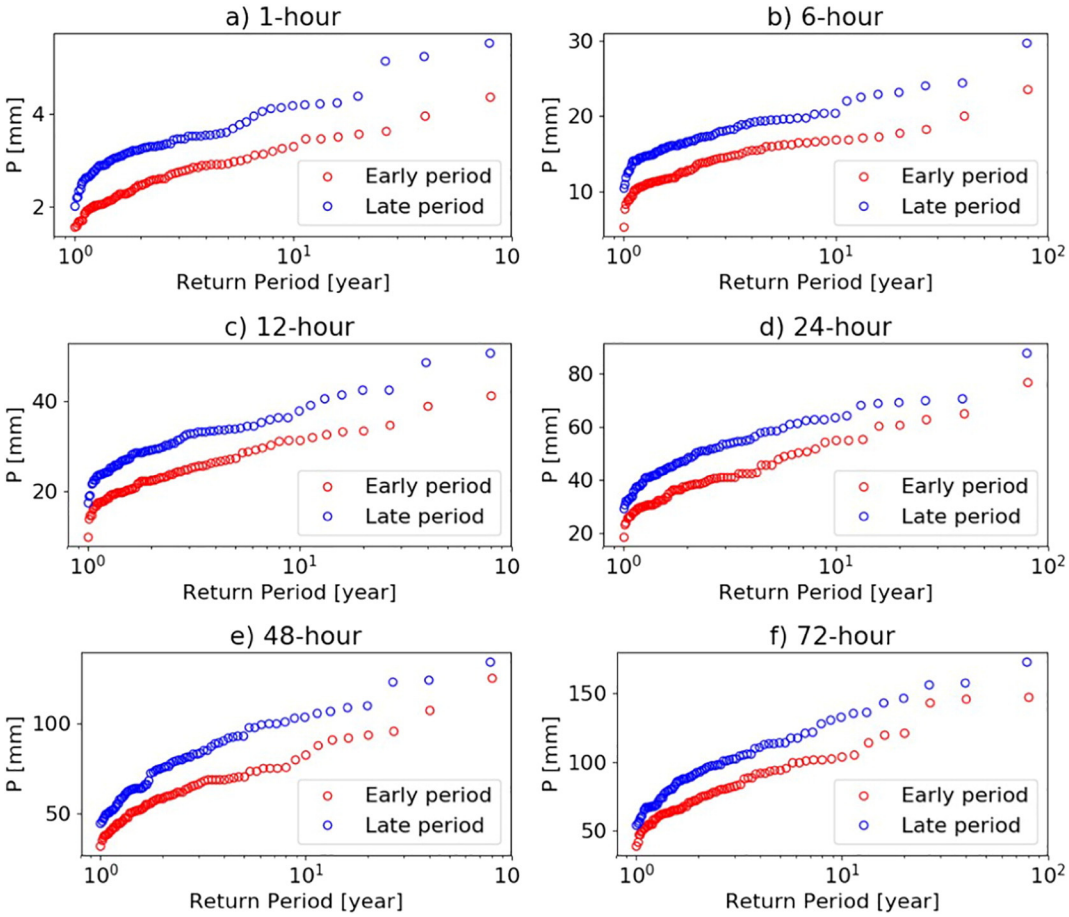

Fig. 7. Frequency distributions of annual maximum 1, 6, 12, 24, 48, and 72-hour basin-average precipitation over the Shasta Dam Watershed. Blue represents the early period (water years 1852 to 1931) and red represents the late period (water years 1932 to 2010).

which indicates that shorter duration storms have a stronger upward trend.

Fig. 7 shows the frequency distributions of annual maximum 1, 6, 12, 24, 48, and 72-hour basin-average precipitation. To ascertain trends in the intensity and temporality of precipitation for each duration of storm events, a decision was made to divide the total historical period in two. The period was split into water years 1852–1931 representing early period, and water years 1932–2010 representing late period. As arbitrary as the time separation might seem, none of the early period precipitation depths exceed the corresponding late period precipitation depths, as seen in every plot in Fig. 7. This behavior indicates more intense precipitation events over SDW in the late historical period than the early period.

To detect the potential trend change time locations in annual maximum 1, 6, 12, 24, 48, and 72-hour basin-average precipitation, the sequential Mann-Kendall test is conducted on each time interval as presented in Fig. 8. Compared with annual precipitation (Fig. 5b), the growths of the progressive series are relatively slow and they show temporal drops around 1900. With respect to 72-hour maximums, the increasing trend from water year 1852 becomes significant only after 1936. However, the progressive series are growing overall throughout the whole period. The retrograde rank series exhibit, on the other hand, stable conditions in recent years, similar to the annual precipitation case. All series show abrupt changes during 1950 to 1960, indicating the increasing trends transit around that period.

The mountainous topography of SDW greatly influences the spatial structure of precipitation. Since precipitation data is obtained at 3 km spatial resolution by the dynamical downscaling method, we further study the spatial variability of trends over SDW. Fig. 9 depicts how the trends over 1852–2010 vary within the watershed. Since there are uncertainties in sub-daily precipitation in a grid-scale, the trend of annual maximum 48-hour precipitation is only shown as the representative of extreme precipitation. In most of the region, annual precipitation and annual maximum 48-hour precipitation have increased by 0.275–0.350% and 0.200–0.350% per year from 1852 to 2010, respectively, which follow the trends of basin-average values provided in Tables 2 and 3. Higher percentage changes can be observed in mountainous regions in the northwest edge and the south edge of the watershed where the mean over the whole period is also high (Fig. 10). This indicates that the wet region has a stronger increasing trend in terms of the percentage change.

The trend in the variability of annual precipitation is analyzed. Fig. 11b shows the time series of the 30-year variance of annual precipitation and the contributions from the wettest and remaining days. The wettest days are defined as the upper 95th percentile of all wet days in the 1852–2010 period following Dettinger (2016). The critical value that separates the wettest 5% days and the remaining 95% days is found to be 14.1 mm/day over SDW. As can be seen from Fig. 11a, the contribution of the remaining days to annual precipitation is rather constant over time, and that of the wettest days fluctuates significantly. The variability of annual precipitation notably increases from 1970s and passes over the historical maximum. The increase in the covariance of the two contributions (green bars) indicates the two contributions are changing more in phase. Thus, while the contribution of the remaining days was relatively constant in the past, it has fluctuated recently along with the contribution of the wettest days. This phenomenon results in dry years becoming drier and wet years becoming wetter.

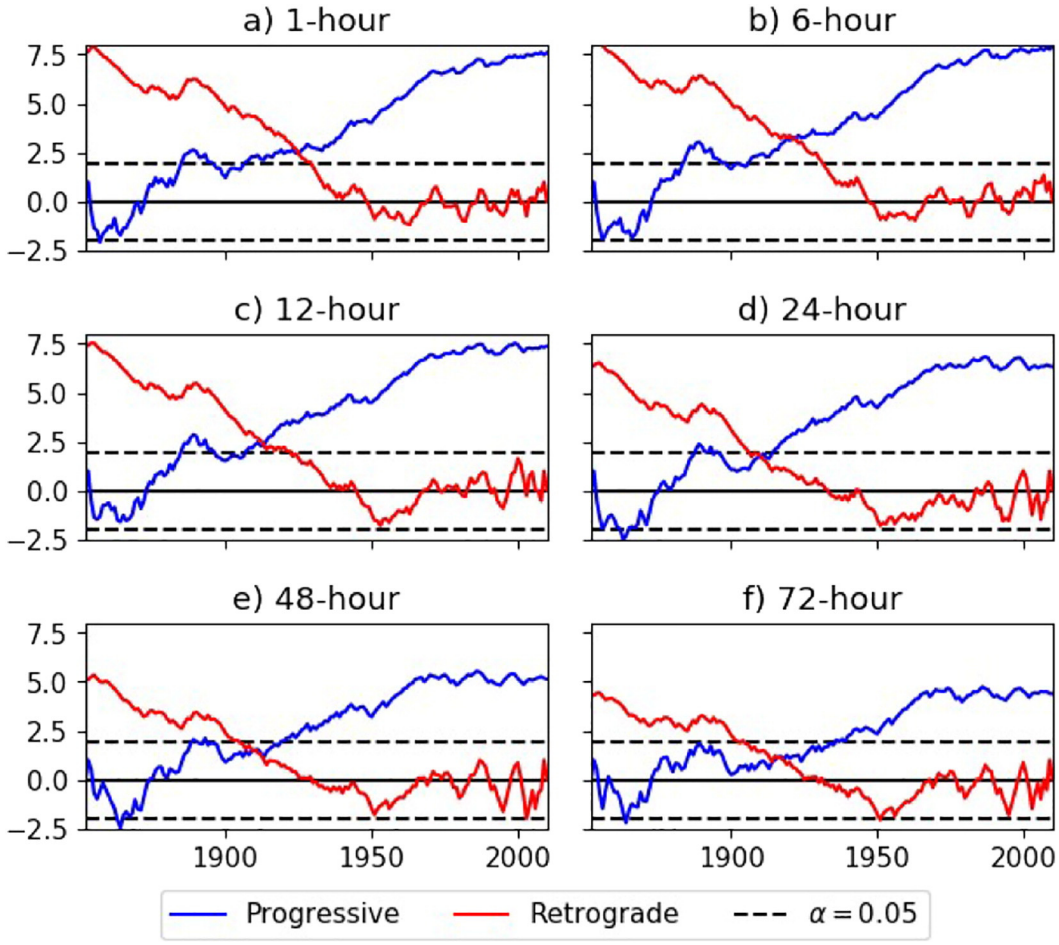

Fig. 8. The sequential Mann-Kendall test on annual maximum 1, 6, 12, 24, 48, and 72-hour basin-average precipitation. Blue and red lines show the progressive and retrograde rank series, respectively. Dashed line corresponds to the 0.05 significance level.

5. Discussion

From a comparison of the model simulation against PRISM observation, at both the daily and monthly timescale, the WRF model-simulated values of basin-average precipitation are consistently higher than those of the PRISM data. Rather than an overestimation by the WRF model, this phenomenon may represent an underestimation of basin-average precipitation in the PRISM dataset over SDW. PRISM is an interpolated dataset where in-situ point measurements at rain gauges are fed into a weighted regression scheme to produce gridded data at a finer scale than the corresponding original observations. One possibility for the underestimation of precipitation by PRISM is the lack of enough rain gauges in SDW to properly interpolate the results over the entire watershed. In complex terrain such as SDW, rain gauges are typically placed in narrow valleys or on relatively flat surfaces (Fig. 1). Fig. 10 also shows that the WRF model produces higher precipitation in a mountainous area. Hence, there is a distinct possibility that the orographic effect causes an underestimation of precipitation in SDW in the PRISM dataset,

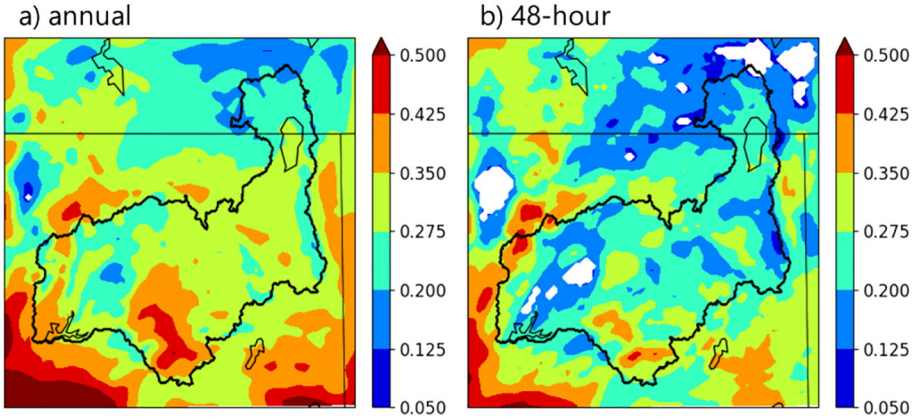

Fig. 9. Spatial distributions of trends in percentage [%/yr] of a) annual precipitation and b) annual maximum 48-hour precipitation over 1852–2010. Trends are expressed as a percentage change of the mean of the whole period in each grid point. Trends with the 0.05 significance level are shown only.

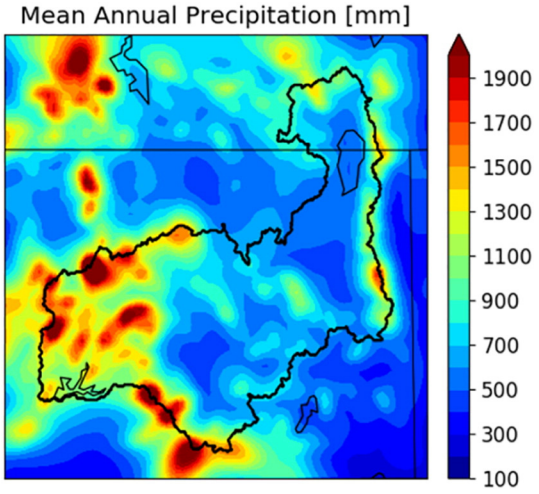

Fig. 10. Mean annual precipitation in water years 1852–2010 obtained by the dynamical downscaling method.

though systematic biases in regional climate models could contribute to uncertainties in this study.

It should be noted that while regional climate models are becoming more reliable in estimating daily precipitation, the quality of sub-daily precipitation is still not adequate (Westra et al., 2014). Particularly, the hourly simulation results should be interpreted with caution. One rationale for our hourly analysis is that we have used basin-average values instead of using 4 km gridded precipitation data directly. We believe that this work provides an appropriate first estimate of the trends of sub-daily extreme precipitation at SDW for the historical period of 159 years, which would be difficult to obtain from pure instrumental records.

We have found that 48-hour extreme precipitation is increasing from 1852 to 2010. The increasing trend is statistically significant for any subseries starting before 1904 to 2010 (from the retrograde rank series in Fig. 8e). Intriguingly, this result contradicts with the regional studies over the west coast of the United States. Kunkel et al. (2013) identified no significant trends in 2-day extreme precipitation over the period of 1895 to 2010 in the Northwest ($p > 0.05, \tau = -0.006$) and the Southwest ($p > 0.05, \tau = 0.012$) regions of the United States. Although the definition of the extreme is different (Kunkel et al. (2013) used 2-day precipitation exceeding a threshold for a 5-year return period), annual maximum 48-hour basin-average precipitation over SDW over the same period is increasing at a 0.01 significance level ($p = 2.24 \times 10^{-3}, \tau = 0.192$). Furthermore, our results differ from a statistically significant declining trend in 2-day extreme precipitation during 1950–2009 in the region from northern California to the central Oregon coast found by Mass et al. (2011) (the extremes are defined as top 60, 40, and 20 events in the 60 year period in this study). These findings suggest that we cannot directly apply the trends found at the regional scale to the watershed-scale, thereby indicating the importance of conducting trend analysis on extreme precipitation at the watershed-scale.

In California, rising temperature, decreasing snowpack, and earlier snow pack are generally found as indicators of change in climate (Cordero et al., 2011; Mote et al., 2005; Stewart et al., 2005). These changes would result in the reduction in summer streamflow, which could then reduce irrigation water, increase water pollution, and increase wild fire (Westerling, 2006). However, the variability of precipitation from year to year in California is probably the most important factor for floods and droughts in California (Dettinger, 2016; Mao et al., 2015), as was witnessed the extreme wet year in 2017 right after a decade of significantly dry years (California Department of Water Resources, 2017, 2015). The increase in the variance of annual precipitation during the recent period (Fig. 11b) implies an increase in the occurrence of extreme dry/wet conditions over SDW. As a result, the integrated management of surface water, dam storage, and groundwater would become more crucial to sustain the water supply to whole California.

Many avenues exist for further analysis using the reconstructed data generated by this study because a regional atmospheric model can produce various variables at each grid point at a fine temporal resolution. For example, if the reconstructed data generated by this study are used as inputs to a hydrologic model, insights into historical streamflow patterns can be provided. The reconstruction of a long-term streamflow record for SDW could yield validation of other streamflow datasets, and provide insights into historical flooding in northern California.

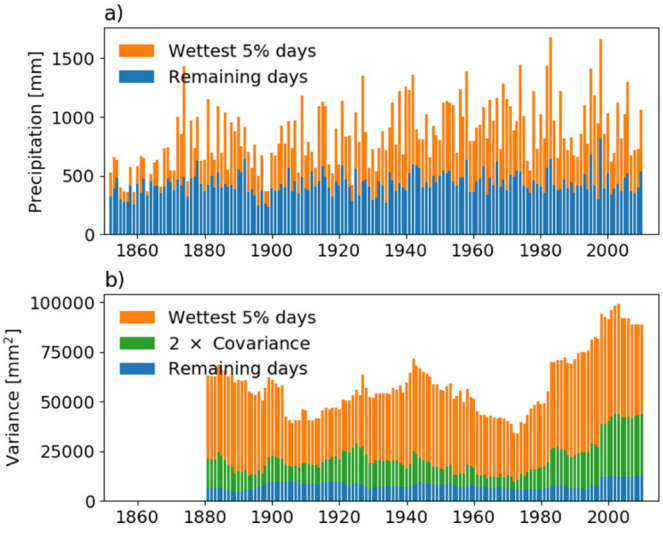

Fig. 11. a) Contributions to annual basin-average precipitation from the upper 95th percentile of wet days (orange) and remaining days (blue) during water years 1852–2010. b) Variances of contributions from the upper 95th percentile of wet days (orange) and remaining days (blue) for the previous 30-years. Green bars are two times the covariance of the two contributions. The total of the three components represents the 30-year variance of annual precipitation.

6. Conclusions

In this study, it was demonstrated that precipitation data derived from historical reconstruction over SDW using dynamical downscaling indicates trends in both long-term rainfall and extreme event behavior. The Mann-Kendall trend test indicates monotonic upward trends in total precipitation depth and intensity for 1, 6, 12, 24, 48, and 72-hour events over the period of water years 1852 to 2010. In the two periods of 1852–1931 and 1932–2010, frequency distributions of extreme precipitation clearly show changes, suggesting that traditional frequency analysis under the assumption of statistical equilibrium may no longer be valid (Kavvas et al., 2017). To examine the changes in the trends of historical precipitation, we used the sequential Mann-Kendall test. This test revealed that while there is an increasing trend in annual precipitation from 1852 to 1940, no significant trend is found from 1941 to 2010. Similarly, the trend in extreme precipitation changes during 1950 to 1960. The spatial distribution of trends reveals that wet area shows more increase in both annual and extreme precipitation during 1852 to 2010. This study also demonstrated the importance of conducting precipitation trend analysis at the watershed-scale. Furthermore, the implications for the water management over SDW were discussed based on the increasing trend found in the variability of annual precipitation since 1970s. The historical trends found in this study, while not direct projections, can help inform policy decisions regarding water supply and flood control issues surrounding Shasta Dam.

This study's methodology has some implications regarding future studies involving both atmospheric and hydrologic modeling. Dynamical downscaling is able to produce reliable climatic data in sparsely gauged basins, enabling the methods of this study to have broad applicability to watersheds around the world. Many of the areas projected to be most affected by climate change are in developing nations, where availability of rainfall data is not as widespread as it is in the United States. This methodology, coupled with GCM projections, could be used to evaluate precipitation trends in regions most vulnerable to climate change impacts. As computing power grows and our understanding of the climate is further refined, the use of regional atmospheric models to recognize trends and predict future behavior will be extremely useful in anticipating the effects of climate change.

Acknowledgments

This study was supported by the California Department of Water Resources (460001378).

References

Alexander, L.V., Zhang, X., Peterson, T.C., Caesar, J., Gleason, B., Klein Tank, A.M.G., Haylock, M., Collins, D., Trewin, B., Rahimzadeh, F., Tagipour, A., Rupa Kumar, K., Revadekar, J., Griffiths, G., Vincent, L., Stephenson, D.B., Burn, J., Aguilar, E., Brunet, M., Taylor, M., New, M., Zhai, P., Rusticucci, M., Vazquez-Aguirre, J.L., 2006. Global observed changes in daily climate extremes of temperature and precipitation. J. Geophys. Res. 111, D05109. https://doi.org/10.1029/2005JD006290.

Bougeault, P., Lacarrere, P., 1989. Parameterization of orography-induced turbulence in a Mesobeta—scale model. Mon. Weather Rev. 117:1872–1890. https://doi.org/10.1175/1520-0493(1989)117<1872:POOITI>2.0.CO;2.

California Department of Water Resources, 2015. California's Most Significant Droughts: Comparing Historical and Recent Conditions. :p. 126 https://doi.org/10.1007/s13398-014-0173-7.2.

California Department of Water Resources, 2017. Water Year 2017: What a Difference a Year Makes 11.

Chen, Z.Q., Kavvas, M.L., Fukami, K., Yoshitani, J., Matsuura, T., 2004. Watershed environmental hydrology (WEHY) model: model application. J. Hydrol. Eng. 9:480–490. https://doi.org/10.1061/(ASCE)1084-0699(2004)9:6(480).

Cheung, W.H., Senay, G.B., Singh, A., 2008. Trends and spatial distribution of annual and seasonal rainfall in Ethiopia. Int. J. Climatol. 28:1723–1734. https://doi.org/10.1002/joc.1623.

Chou, M., Suarez, M.J., 1999. A Solar Radiation Parameterization for Atmospheric Studies.

Compo, G.P., Whitaker, J.S., Sardeshmukh, P.D., Matsui, N., Allan, R.J., Yin, X., Gleason, B.E., Vose, R.S., Rutledge, G., Bessemoulin, P., Brönnimann, S., Brunet, M., Crouthamel, R.I., Grant, A.N., Groisman, P.Y., Jones, P.D., Kruk, M.C., Kruger, A.C., Marshall, G.J., Maugeri, M., Mok, H.Y., Nordli, Ø., Ross, T.F., Trigo, R.M., Wang, X.L., Woodruff, S.D., Worley, S.J., 2011. The twentieth century reanalysis project. Q. J. R. Meteorol. Soc. 137:1–28. https://doi.org/10.1002/qj.776.

Cordero, E.C., Kessomkiat, W., Abatzoglou, J., Mauget, S.A., 2011. The identification of distinct patterns in California temperature trends. Clim. Chang. 108:357–382. https://doi.org/10.1007/s10584-011-0023-y.

Daly, C., Halbleib, M., Smith, J.I., Gibson, W.P., Doggett, M.K., Taylor, G.H., Curtis, J., Pasteris, P.P., 2008. Physiographically sensitive mapping of climatological temperature and precipitation across the conterminous United States. Int. J. Climatol. 28:2031–2064. https://doi.org/10.1002/joc.1688.

Dettinger, M., 2016. Historical and Future Relations Between Large Storms and Droughts in California. San Fr. Estuary Watershed Sci. 14, Article 1. https://doi.org/10.15447/sfews.2016v14iss2art2.

Dettinger, M.D., Ralph, F.M., Das, T., Neiman, P.J., Cayan, D.R., 2011. Atmospheric rivers, floods and the water resources of California. Water 3:445–478. https://doi.org/10.3390/w3020445.

Dore, M.H.I., 2005. Climate change and changes in global precipitation patterns: what do we know? Environ. Int. 31:1167–1181. https://doi.org/10.1016/j.envint.2005.03.004.

Engstrom, W.N., 1996. The California storm of January 1862. Quat. Res. 46:141–148. https://doi.org/10.1006/qres.1996.0054.

Grell, G., Dudhia, J., Stauffer, D.R., 1994. A Description of the Fifth-generation Penn State/NCAR Mesoscale Model (MM5). NCAR Tech. Note NCAR/TN-398+STR 121. https://doi.org/10.5065/D60Z716B.

Groisman, P.Y., Knight, R.W., Easterling, D.R., Karl, T.R., Hegerl, G.C., Razuvaev, V.N., 2005. Trends in intense precipitation in the climate record. J. Clim. 18:1326–1350. https://doi.org/10.1175/JCLI3339.1.

Halpert, M.S., Bell, G.D., 1997. Climate assessment for 1996. Bull. Am. Meteorol. Soc. 78. https://doi.org/10.1175/1520-0477(1997)078<1038:CAF>2.0.CO;2 (1038–1038).

Han, J., Pan, H.-L., 2011. Revision of convection and vertical diffusion schemes in the NCEP global forecast system. Weather Forecast. 26:520–533. https://doi.org/10.1175/WAF-D-10-05038.1.

Higgins, R.W., Silva, V.B.S., Shi, W., Larson, J., 2007. Relationships between climate variability and fluctuations in daily precipitation over the United States. J. Clim. 20:3561–3579. https://doi.org/10.1175/JCLI4196.1.

Ishida, K., Kavvas, M.L., 2016. Climate change analysis on historical watershed-scale precipitation by means of long-term dynamical downscaling. Hydrol. Process. https://doi.org/10.1002/hyp.10932.

Ishida, K., Gorguner, M., Ercan, A., Trinh, T., Kavvas, M.L., 2017. Trend analysis of watershed-scale precipitation over Northern California by means of dynamically-downscaled CMIP5 future climate projections. Sci. Total Environ. 592:12–24. https://doi.org/10.1016/j.scitotenv.2017.03.086.

Kanamitsu, M., Kumar, A., Juang, H.M.H., Schemm, J.K., Wang, W., Yang, F., Hong, S.Y., Peng, P., Chen, W., Moorthi, S., Ji, M., 2002. NCEP dynamical seasonal forecast system 2000. Bull. Am. Meteorol. Soc. 83:1019–1037. https://doi.org/10.1175/1520-0477(2002)083<1019:NDSFS>2.3.CO;2.

Karl, T.R., Knight, R.W., 1998. Secular trends of precipitation amount, frequency, and intensity in the United States. Bull. Am. Meteorol. Soc. 79:231–241. https://doi.org/10.1175/1520-0477(1998)079<0231:STOPAF>2.0.CO;2.

Kavvas, M.L., Chen, Z.Q., Dogrul, C., Yoon, J.Y., Ohara, N., Liang, L., Aksoy, H., Anderson, M.L., Yoshitani, J., Fukami, K., Matsuura, T., 2004. Watershed environmental hydrology (WEHY) model based on upscaled conservation equations: hydrologic module. J. Hydrol. Eng. 9:450–464. https://doi.org/10.1061/(ASCE)1084-0699(2004)9:6(450).

Kavvas, M.L., Kure, S., Chen, Z.Q., Ohara, N., Jang, S., 2012. WEHY-HCM for modeling interactive atmospheric-hydrologic processes at watershed scale: I. Model description. J. Hydrol. Eng. 121001112817009. https://doi.org/10.1061/(ASCE)HE.1943-5584.0000724.

Kavvas, M.L., Ishida, K., Trinh, T., Ercan, A., Darama, Y., Carr, K.J., 2017. Current issues in and an emerging method for flood frequency analysis under changing climate. Hydrol. Res. Lett. 11:1–5. https://doi.org/10.3178/hrl.11.1.

Kendall, M., 1948. Rank Correlation Methods.

Kiely, G., 1999. Climate change in Ireland from precipitation and streamflow observations. Adv. Water Resour. 23:141–151. https://doi.org/10.1016/S0309-1708(99)00018-4.

Kunkel, K.E., Karl, T.R., Brooks, H., Kossin, J., Lawrimore, J.H., Arndt, D., Bosart, L., Changnon, D., Cutter, S.L., Doesken, N., Emanuel, K., Groisman, P.Y., Katz, R.W., Knutson, T., O'Brien, J., Paciorek, C.J., Peterson, T.C., Redmond, K., Robinson, D., Trapp, J., Vose, R., Weaver, S., Wehner, M., Wolter, K., Wuebbles, D., 2013. Monitoring and understanding trends in extreme storms: state of knowledge. Bull. Am. Meteorol. Soc. 94:499–514. https://doi.org/10.1175/BAMS-D-11-00262.1.

Kure, S., Jang, S., Ohara, N., Kavvas, M.L., Chen, Z.Q., 2013. WEHY-HCM for modeling interactive atmospheric-hydrologic processes at watershed scale. II: model application to ungauged and sparsely gauged watersheds. J. Hydrol. Eng. 18:1272–1281. https://doi.org/10.1061/(ASCE)HE.1943-5584.0000701.

Lin, Y., Colle, B.a., 2011. A new bulk microphysical scheme that includes riming intensity and temperature-dependent ice characteristics. Mon. Weather Rev. 139:1013–1035. https://doi.org/10.1175/2010MWR3293.1.

Mann, H.B., 1945. Nonparametric tests against trend. Econometrica 13:245. https://doi.org/10.2307/1907187.

Mao, Y., Nijssen, B., Lettenmaier, D.P., 2015. Is climate change implicated in the 2013–2014 California drought? A hydrologic perspective. Geophys. Res. Lett. 42:2805–2813. https://doi.org/10.1002/2015GL063456.

Maraun, D., Wetterhall, F., Ireson, A.M., Chandler, R.E., Kendon, E.J., Widmann, M., Brienen, S., Rust, H.W., Sauter, T., Themeßl, M., Venema, V.K.C., Chun, K.P., Goodess, C.M., Jones, R.G., Onof, C., Vrac, M., Thiele-Eich, I., 2010. Precipitation downscaling under climate change: recent developments to bridge the gap between dynamical models and the end user. Rev. Geophys. 48, RG3003. https://doi.org/10.1029/2009RG000314.

Mass, C., Skalenakis, A., Warner, M., 2011. Extreme precipitation over the west coast of North America: is there a trend? J. Hydrometeorol. 12:310–318. https://doi.org/10.1175/2010JHM1341.1.

Min, S.-K., Zhang, X., Zwiers, F.W., Hegerl, G.C., 2011. Human contribution to more-intense precipitation extremes. Nature 470:378–381. https://doi.org/10.1038/nature09763.

Mote, P.W., Hamlet, A.F., Clark, M.P., Lettenmaier, D.P., 2005. Declining mountain snowpack in western north America*. Bull. Am. Meteorol. Soc. 86:39–49. https://doi.org/10.1175/BAMS-86-1-39.

Niu, G.Y., Yang, Z.L., Mitchell, K.E., Chen, F., Ek, M.B., Barlage, M., Kumar, A., Manning, K., Niyogi, D., Rosero, E., Tewari, M., Xia, Y., 2011. The community Noah land surface model with multiparameterization options (Noah-MP): 1. Model description and evaluation with local-scale measurements. J. Geophys. Res. Atmos. 116:1–19. https://doi.org/10.1029/2010JD015139.

O'Gorman, P.A., 2015. Precipitation extremes under climate change. Curr. Clim. Chang. Rep. 1:49–59. https://doi.org/10.1007/s40641-015-0009-3.

Pryor, S.C., Howe, J.A., Kunkel, K.E., 2009. How spatially coherent and statistically robust are temporal changes in extreme precipitation in the contiguous USA? Int. J. Climatol. 29:31–45. https://doi.org/10.1002/joc.1696.

Ralph, F.M., Neiman, P.J., Wick, G.A., Gutman, S.I., Dettinger, M.D., Cayan, D.R., White, A.B., 2006. Flooding on California's Russian River: role of atmospheric rivers. Geophys. Res. Lett. 33, L13801. https://doi.org/10.1029/2006GL026689.

Sachindra, D.A., Huang, F., Barton, A., Perera, B.J.C., 2014. Statistical downscaling of general circulation model outputs to precipitation-part 2: bias-correction and future projections. Int. J. Climatol. 34:3282–3303. https://doi.org/10.1002/joc.3915.

Saha, S., Nadiga, S., Thiaw, C., Wang, J., Wang, W., Zhang, Q., Van den Dool, H.M., Pan, H.-L., Moorthi, S., Behringer, D., Stokes, D., Peña, M., Lord, S., White, G., Ebisuzaki, W., Peng, P., Xie, P., 2006. The NCEP climate forecast system. J. Clim. 19:3483–3517. https://doi.org/10.1175/JCLI3812.1.

Saidi, H., Ciampittiello, M., Dresti, C., Ghiglieri, G., 2013. The climatic characteristics of extreme precipitations for short-term intervals in the watershed of Lake Maggiore. Theor. Appl. Climatol. 113:1–15. https://doi.org/10.1007/s00704-012-0768-x.

Schär, C., Ban, N., Fischer, E.M., Rajczak, J., Schmidli, J., Frei, C., Giorgi, F., Karl, T.R., Kendon, E.J., Tank, A.M.G.K., O'Gorman, P.A., Sillmann, J., Zhang, X., Zwiers, F.W., 2016. Percentile indices for assessing changes in heavy precipitation events. Clim. Chang. 137:201–216. https://doi.org/10.1007/s10584-016-1669-2.

Sen, P.K., 1968. Estimates of the regression coefficient based on Kendall's Tau. J. Am. Stat. Assoc. 63:1379. https://doi.org/10.2307/2285891.

Skamarock, W.C., Klemp, J.B., Dudhi, J., Gill, D.O., Barker, D.M., Duda, M.G., Huang, X.-Y., Wang, W., Powers, J.G., 2008. A description of the advanced research WRF version 3. Tech. Rep. 113. https://doi.org/10.5065/D68S4MVH.

Sneyers, R., Tuomenvirta, H., Heino, R., 1998. Observations in homogeneities and detection of climate change. Geophysica 34, 159–178.

Stewart, I.T., Cayan, D.R., Dettinger, M.D., 2005. Changes toward earlier streamflow timing across western north America. J. Clim. 18:1136–1155. https://doi.org/10.1175/JCLI3321.1.

Toride, K., Cawthorne, D.L., Ishida, K., Diaz, A.J., Kavvas, L.M., Anderson, M.L., 2017a. Climate change trend analysis on extreme precipitation over the Shasta Dam watershed based on 159-year long-term dynamic downscaling. World Environmental and Water Resources Congress 2017. American Society of Civil Engineers, Reston, VA: pp. 427–436 https://doi.org/10.1061/9780784480618.043.

Toride, K., Ishida, K., Kavvas, L.M., Anderson, M.L., 2017b. Maximum precipitation estimation over Shasta Dam watershed by means of atmospheric boundary condition shifting method. World Environmental and Water Resources Congress 2017. American Society of Civil Engineers, Reston, VA:pp. 340–346 https://doi.org/10.1061/9780784480618.033.

Toride, K., Neluwala, P., Kim, H., Yoshimura, K., 2017c. Feasibility study of the reconstruction of historical weather with data assimilation. Mon. Weather Rev. 145:3563–3580. https://doi.org/10.1175/MWR-D-16-0288.1.

Trinh, T., Jang, S., Ishida, K., Ohara, N., Chen, Z.Q., Anderson, M.L., Darama, Y., Chen, J., Kavvas, M.L., 2016. Reconstruction of historical inflows into and water supply from Shasta Dam by coupling physically based hydroclimate model with reservoir operation model. J. Hydrol. Eng. 21:1–12. https://doi.org/10.1061/(ASCE)HE.1943-5584.0001391.

Trinh, T., Ishida, K., Kavvas, M.L., Ercan, A., Carr, K., 2017a. Assessment of 21st century drought conditions at Shasta Dam based on dynamically projected water supply conditions by a regional climate model coupled with a physically-based hydrology model. Sci. Total Environ. 586:197–205. https://doi.org/10.1016/j.scitotenv.2017.01.202.

Trinh, T., Kavvas, M.L., Ishida, K., Carr, K., Ohara, N., 2017b. Projected 21st century climate change on snow conditions over Shasta dam watershed by means of dynamical downscaling. Hydrol. Process. 31:2887–2901. https://doi.org/10.1002/hyp.11231.

Villarini, G., Serinaldi, F., Smith, J.A., Krajewski, W.F., 2009. On the stationarity of annual flood peaks in the continental United States during the 20th century. Water Resour. Res. 45:1–17. https://doi.org/10.1029/2008WR007645.

Westerling, A.L., 2006. Warming and earlier spring increase western U.S. forest wildfire activity. Science 313:940–943 (80-.). https://doi.org/10.1126/science.1128834.

Westra, S., Alexander, L.V., Zwiers, F.W., 2013. Global increasing trends in annual maximum daily precipitation. J. Clim. 26:3904–3918. https://doi.org/10.1175/JCLI-D-12-00502.1.

Westra, S., Fowler, H.J., Evans, J.P., Alexander, L.V., Berg, P., Johnson, F., Kendon, E.J., Lenderink, G., Roberts, N.M., 2014. Future changes to the intensity and frequency of short-duration extreme rainfall. Rev. Geophys. 52:522–555. https://doi.org/10.1002/2014RG000464.

Zhu, Y., Newell, R.E., 1998. A proposed algorithm for moisture fluxes from atmospheric rivers. Mon. Weather Rev. 126:725–735. https://doi.org/10.1175/1520-0493(1998)126<0725:APAFMF>2.0.CO;2.